Hindawi
Journal of Nanomaterials
Volume 2022, Article ID 2188705, 15 pages
https://doi.org/10.1155/2022/2188705

Research Article

Multiobjective Optimization of EDM Parameters for Rice Husk Ash/Cu/Mg-Reinforced Hybrid Al-0.7Fe-0.6Si-0.375Cr-0.25Zn Metal Matrix Nanocomposites for Engineering Applications: Fabrication and Morphological Analysis

Ram Narayan Muni,[1] Jujhar Singh,[2] Vineet Kumar,[3] Shubham Sharma,[2,4,5] P. Sudhakara,[4] Vivek Aggarwal,[2] and S. Rajkumar[6]

[1]*Research Scholar, Dept. of Mechanical Engg., IKGPTU, Kapurthala, 144603 Jalandhar, Punjab, India*
[2]*Department of Mechanical Engineering, IKGPTU, Main Campus, Kapurthala, 144603 Jalandhar, Punjab, India*
[3]*Department of Automobile Engineering, Chandigarh University, Gharuan, 140413 Mohali, Punjab, India*
[4]*CSIR-Central Leather Research Institute, Regional Centre-Jalandhar, 144021 Punjab, India*
[5]*Department of Mechanical Engineering, University Centre for Research and Development, Chandigarh University, 140413 Punjab, India*
[6]*Department of Mechanical Engineering, Faculty of Manufacturing, Institute of Technology, Hawassa University, Ethiopia*

Correspondence should be addressed to Jujhar Singh; jujharsingh2085@gmail.com and S. Rajkumar; rajkumar@hu.edu.et

Received 8 November 2021; Revised 21 January 2022; Accepted 15 March 2022; Published 31 March 2022

Academic Editor: Palanivel Velmurugan

The advanced class of Al/(RHA+Mg+Cu) hybrid metal matrix nanocomposites (MMNCs) has exhibited superior physical, and mechanical properties with superior wettability and chemical compatibility. This work has also been reported on the machining and multiobjective optimization of process variables for the machining of Al/(RHA+Mg+Cu) hybrid MMNCs on EDM using L_{27} Taguchi's orthogonal array integrated with Grey rational analysis (GRA). The primarily target goal of this study is to produce nanocomposite having better properties with minimal production cost, with the use of reinforcement rice husk ash (RHA). RHA is utilized in the base matrix of Al 6061 at wt.% of 6, 8, and 10. On the other hand, the elements such as Cu and Mg are placed fixed, i.e., 3 wt.% and 1 wt.%, respectively. The hardness, tensile strength, and impact strength of the nanocomposites increased with the maximum increment of 35.11%, 15.76%, and 16.67%, respectively, as compared to neat composite. Further, the purpose of this investigation was to determine the effect of various factors such as the percentage of RHA in the workpiece electrode (W), the discharge current (I), the voltage (V), the duty factor (τ), the pulse-on time (Ton), and the flushing pressure (P) on the material removal rate (MRR), the surface roughness (SR), and the tool wear rate (TWR) during the machining of hybrid nanocomposites using Taguchi's approach. The results revealed that MRR decreased with increasing the RHA content in the workpiece which can be reasoned to isolating nature of the RHA. It clearly shows that SR has decreased with an addition of RHA content from 6 wt.% to 8 wt.% in workpiece, but it slightly increased by further addition of RHA from 8 wt.% to 10 wt.%. SR has decreased with an increase in duty factor while performing EDM trials with the copper electrode, but it slightly increases with a further increase in duty factor. By the increase in pulse-on time, spark energy also increases also leading to the formation of craters. Therefore, SR has increased with an increase in pulse-on time. The TWR has increased with an increase in RHA content in the workpiece, because of the existence of hard reinforcements on the matrix which causes larger wear in the tool. Analysis of SEM micrographs showed the presence of voids, shallow and deep craters, and black voids on the machined surface of the fabricated hybrid nanocomposites. As calculated using the response graph for GRG, confirmation tests for optimal parametric setting show improvement over initial parametric setting of machining parameters. The mean of optimal MRR, SR, and TWR is estimated at the significant level of machining factors at $A_1B_3C_3D_2E_3F_1$, $A_2B_1C_1D_2E_1F_3$, and $A_1B_1C_1D_1E_1F_3$, respectively.

1. Introduction

The metal composite matrix (MMCs) can be processed by various methods, such as water jet drilling, turning, cutting, abrasive water jet machining, and laser cutting. However, such methods have some limitations in cutting complex profiles [1, 2]. EDM is more able to cut complex forms with high accuracy and control for such composites. But many problems and difficulties have been faced by the manufacturing engineers during processing of the composite materials which include rapid tool wear, irregular MRR, and poor surface finish. Till date, very little research work is done to test the machinability of RHA-reinforced MMCs to recommend the optimum range of the machining parameters for the practical use in the industry. The choice of suitable machining parameters is generally difficult and depends largely on the operator knowledge and tables of input process variables given by the machine tool manufacturer. Therefore, optimization of process variables is quite essential when the economy and performance of a machined component contribute [3, 4]. Bhoi et al. reviewed the fabrication of Al matrix composites reinforced by micro-/nanoparticles [4]. Alaneme and Olubambi observed that the coefficient of friction and the wear rate of the composites were increased with increase in RHA wt.% [5]. Shaikh et al. investigated the characteristics of newly developed aluminium matrix composites reinforced with 0, 5, 10, and 15 wt.% RHA and 10 wt.% of SiC. Dry sliding wear, density, hardness, and porosity were evaluated for the produced composites. Except for 15 wt.% of the RHA composite where clustering of RHA particles is found, SEM micrographs showed a uniform dispersion of SiC and RHA particles in the developed composite. The mechanical and tribological analysis showed that the hardness and wear characteristics of composites were first increased and then decreased up to 10 percentages by increasing the RHA percentage [6]. Mishra P. et al. developed the new MMC using aluminium alloy (LM6) matrix reinforced with 6 wt.% RHA using stir casting technique and examined the properties such as hardness and wear properties [7]. Zakaria investigated the microstructure and corrosion behaviour of Al/SiC metal matrix composites [8]. Hossain et al. fabricated aluminium matrix hybrid composites reinforced with 1 wt.% Al_2O_3 and 0, 2, 4, 6, and 8 wt.% SiC by stir casting technique and examined mechanical, wear, and microstructural characteristics [9]. Sharma et al. examined the different fabrication techniques along with the different reinforcements used in the newly fabricated MMCs [10]. Sharma et al. also investigated the mechanical, tribological, and microstructural properties of Al-Mg-Si-T6/SiC/muscovite hybrid metal matrix composites for high strength applications [11]. Dinaharan et al. fabricated the 18 vol% RHA-reinforced AA6061 matrix composite using friction-stir processing. The developed composite offered a fine and equiaxed grain structure with an increase in tensile strength [12]. Srivastava focused on the construction of an aluminium 6063 matrix composite reinforced with 5% SiC (30 mm in size). The result showed that the produced MMC improved toughness and strength. Further studied effectiveness of MMC produced using EDM. The results showed that all the factors significantly were affecting the results of MRR [13]. A review of literature found that while there has been work on machining single particle reinforced MMC on EDM, there has been very little work on machining the Al matrix hybrid composites reinforced with RHA, magnesium, and copper. In the present investigation, Taguchi method-based design of experiments and Grey relational analysis identify the optimal combinations using single response and multiresponse optimization, respectively, during EDM of newly fabricated RHA-reinforced Al matrix nanocomposites.

2. Experimental Procedure

2.1. Material Selection. Matrix and reinforcement selection is the backbone of every composite for enhancement in the properties. In this nanocomposites, Al 6061 alloy is employed as the matrix, whereas RHA, Cu, and Mg are used as reinforcements. Al 6061 contains Mg and Si as its primary alloying elements. It is one of the most widely utilized aluminium alloys in series 6000 and has desired mechanical and tribological properties, thermal and electrical conductivity, and high degree of stiffness [14, 15]. In the present work, commercial grade Al 6061 with chemical composition shown in Table 1 is obtained from Bagri Alloy and Steel, Chandigarh.

Compressibility behaviour of Al matrix MMNCs can be enhanced with reinforcing the Cu particles. The improved compressibility is due to the high hardness, high resistance to deformation, and the spherical shape of copper nanoparticles, which are capable of significantly reducing the area of contact between adjacent particles. The addition of copper is based upon its high solubility in aluminium. Copper is also mechanically tougher than pure aluminium. The addition of Cu linearly increases the microhardness. The primary requirement during the fabrication of MMNCs is wetting between the reinforcements and the matrix alloy, particularly fabrication using liquid processing method. The magnesium decreases the surface tension of liquid metal, which thereby overcomes weak bonding in metal matrix and reinforced particles by an increment in wettability.

2.2. Fabrication of Nanocomposites. In this work, 6, 8, and 10 wt.% RHA, 3 wt.% copper, and 1 wt.% magnesium are used as reinforcements, and Al 6061 is selected as matrix material for the nanocomposite's fabrication. Table 2 shows designated samples and their compositions. The composites are prepared using two step stir casting method. The RHA and copper particles were initially preheated separately at a temperature of 250°C to remove moisture and to improve wettability with molten Al alloy in a preheating furnace [18, 19]. The Al alloy was charged in graphite crucible and is melted to a temperature of about 750°C using an electrical furnace [20, 21]. The liquid alloy was cooled in the furnace to a semisolid state at a temperature of about 630°C. The preheated RHA and copper particles were charged into the semisolid melt at this temperature and stirred manually for 20 minutes, and 1 wt.% of magnesium was added to improve the wettability between the matrix and reinforcements [22,

Table 1: Chemical composition of Al 6061 [16, 17].

Manganese	Iron	Copper	Magnesium	Silicon	Zinc	Chromium	Others	Aluminium
0.15%	0.7%	0.23%	0.15%	0.6%	0.25%	0.37%	0.12%	Balance

Table 2: Samples with their wt.% composition.

Sample designation	Composition (wt.%) of hybrid MMNCs
W_1	90%Al6061-6%RHA-3%Cu-1%Mg
W_2	88%Al6061-8%RHA-3%Cu-1%Mg
W_3	86%Al6061-10%RHA-3%Cu-1%Mg

23]. The addition of magnesium enhances the wettability; however, increasing the content above 1 wt.% causes the increase in viscosity of the slurry, and hence, uniform particle distribution might be difficult. For uniform distribution of reinforcement in the matrix, the flow pattern should be from outward to inward [24]. The argon gas was supplied into the crucible during the stirring in order to avoid the formation of an oxide layer on the surface of the matrix melt [25, 26]. The semisolid hybrid composite mixture was heated to a temperature of about 900°C and stirred using an automated mechanical stirrer at 300-400 rpm for 10 minutes [27, 28]. In the end, mixed liquid nanocomposites are poured inside the cavity to produce the casting [29].

2.3. Specimen Preparation. The specimens of aluminium matrix hybrid nanocomposites are prepared as per Table 2 composition as exhibited above. The hardness of the nanocomposites increases with an increase in reinforcements content with the maximum increment of 35.11% for the 10wt.% RHA and 3 wt.% of Cu in comparison with an increment of 17.20% for -6wt.% RHA [30, 31]. The specimens are prepared in a cylindrical shape with a base diameter of 34 mm and a length of 10 mm. The workpieces are machined using copper electrodes made with a diameter of 10 mm. The one set prepared specimen of workpiece and tool is shown in Figure 1. The mechanical properties of aluminium matrix hybrid nanocomposites are presented in Table 3.

2.4. Machining Parameters. The experiments are carried out on a numerically controlled die-sinking EDM machine (5535-ElectraPlus PS-35), as shown in Figure 2. The z-axis motor is controlled by the control panel and can be configured to follow the programme fed to the controller [30, 31]. The control system uses the voltage difference between the tool and the workpiece electrodes to control the tool's position. The tool is fed to keep a constant separation with the workpiece.

Based on the pilot study and extensive literature review, there are 6 factors at 3 levels identified as wt.% of RHA in the workpiece electrode (A), the discharge current (B), gap voltage (C), duty factor (D), pulse-on time (E), and the flushing pressure (F). Table 4 shows the ranges and levels of process parameters selected based on pilot experiments and the availability of the machine.

The performance characteristics include MRR, TWR, and SR. MRR is defined as the ratio of the weight difference of the workpiece prior to machining (Wb) and postmachining (Wa) to the machining time (t):

$$\mathrm{MRR}\left(\frac{\mathrm{g}}{\mathrm{min.}}\right) = \frac{W_b - W_a}{t} \tag{1}$$

Similarly, TWR is determined as the ratio of the tool's weight difference before (Tb) and after (Ta) machining to the time of machining:

$$\mathrm{TWR}\left(\frac{\mathrm{g}}{\mathrm{min.}}\right) = \frac{T_b - T_a}{t} \tag{2}$$

SR is the measure of the fine irregularities observed in the texture of the surface. These are the results of the EDM process employed to create the surface. Generally, the surface roughness is denoted by Ra and expressed in micrometers (μm).

3. Results and Discussions

The SN ratio diagrams are then shown using Minitab 17 software against the resulting response for analysis [32, 33]. In general, there are three categories for evaluating the SN ratio: lower is better (LB), nominal is better (NB), and higher is better (HB), and their selection is determined by the type of response recorded. The HB category is applied for MRR, whereas the LB category is applied for the TWR and SR.

$$\begin{aligned}(S/N)HB &= -10\log_{10}\left[\frac{1}{n}\sum_{i=1}^{n}\frac{1}{y_i^2}\right]\\ (S/N)LB &= -10\log_{10}\left[\frac{1}{n}\sum_{i=1}^{n}y_i^2\right]\end{aligned} \tag{3}$$

where y_i denotes the observed results of the ith experiment of n repetitions.

The experimental results of the MRR, SR, and TWR of sample W_1, W_2, and W_3 of hybrid nanocomposites machined by copper electrodes are presented in Table 5.

3.1. Effect of EDM Parameters on MRR, SR, and TWR. As Table 5 has showed the experiment results with reference to MRR, SR, and TWR and their corresponding SN ratios, the response table of means and S/N ratio for MRR is shown in Table 6, respectively. The variations of MRR, SR, and TWR with respect to different factors while machining the given nanocomposites with the copper electrode are presented in Figures 3, 4, and 5, respectively. It is captured that MRR decreased with increasing the RHA content in

Figure 1: Prepared specimen of the workpiece (diameter 34 mm and thickness 10 mm) and tool electrode (diameter 10 mm).

Table 3: Mechanical characteristics of prepared nanocomposites [30].

Samples	Tensile strength (MPa)	Rockwell-hardness (HRB)	Impact toughness (J)	Elongation-at-break (%)
W_0 (neat Al6061)	85	43	3	9.7
W_1	95.2	54.1	3.5	7.7
W_2	97.1	57	3	6.3
W_3	98.4	58.1	2.5	5.3

workpiece which can be reasoned to isolating nature of the RHA. Rengasamy et al. also claimed that the value of MRR is maximum at 0 wt.% of reinforcement and it reduces gradually with the increase wt.% of reinforcement with matrix alloys [34]. The SN ratio response graphs further show that MRR increases with an increase in discharge current. Discharge energy becomes high at the high level of discharge current as a result of which a large heat transfer occurs to the workpiece which causes high MRR. This has been also claimed by Kandpal et al. (2018) [35]. With an increase in gap voltage, MRR is found to be increased. It is clear that with the increase of discharge current and pulse-on time, the applied pulse energy increases for each discharge. Because of that, high thermal energy is released which is enough to remove the large amounts of material from the workpiece specimen and hence increase the MRR. The analysis also satisfies the claim of Dhar et al. [36]. MRR is maximum at a low level of flushing pressure which could be subjected to the levels of the flushing pressure chosen for machining. From Figure 3, it can be clearly shown that MRR improves with increasing the duty cycle from low level to moderate level; however, MMR is dropped down when the duty cycle is kept at a high level.

The S/N ratio response graphs show the significant effect of reinforcements on SR. It clearly shows that SR decreases with an addition of RHA content from 6 wt.% to 8 wt.% in workpiece, but it slightly increased by further addition of RHA from 8 wt.% to 10 wt.%. Thus, SR value is found minimum at moderate level, i.e., at 8 wt.% of RHA content. The reinforcement particles dislodged from the machine surface are one of the reasons to enhance roughness. The SN ratio response graphs further show that SR leads to an increase with an increase in current. Since discharge energy is high at a higher discharge current, as a result, a large amount of heat is transferred to the workpiece which causes the formation of more craters on the machined surface and leads to poor surface finish. This analysis is also satisfied the claim by Bodukuri et al. [37]. SR is found to increase initially with an increase in gap voltage and then decreases. SR decreases with an increase in duty factor while performing EDM trials with the copper electrode, but it slightly increases with further increase in duty factor.

By the increase in pulse-on time, spark energy also increases that also leads to the formation of craters. Therefore, SR increases with an increase in pulse-on time. It is also identified during machining that the large size craters and further overlapping of craters are done because of the extremely large amount of energy delivered to the workpiece with an increase in pulse-on time and discharge current. SR is noticed to be marginally varying with different level of flushing pressure.

The TWR increases with an increase in RHA content in the workpiece, because of the existence of hard reinforcements on the matrix which causes larger wear in the tool. The SN ratio response graph further shows that TWR increases by increasing the discharge current. The amount of material removed from the tool electrode increases proportionally with an increase in the discharge current. Discharge energy is high at a higher discharge current as a result large amount of heat is produced near the gap, which causes high TWR. TWR also increases with increasing the level of gap voltage for a copper electrode as spark energy is high at high level of gap voltage. TWR also increases with an increase in the duty factor. In this case, TWR is the minimum at a low level of duty factor. By increasing the pulse-on time, spark energy also increases that also leads to higher TWR. TWR initially increases and then decreases for the copper electrode. When the pulse time is higher, the plasma channel continues to expand and can reduce the energy density of the discharge. Hence, TWR declines. TWR is minimum at a high level of flushing pressure.

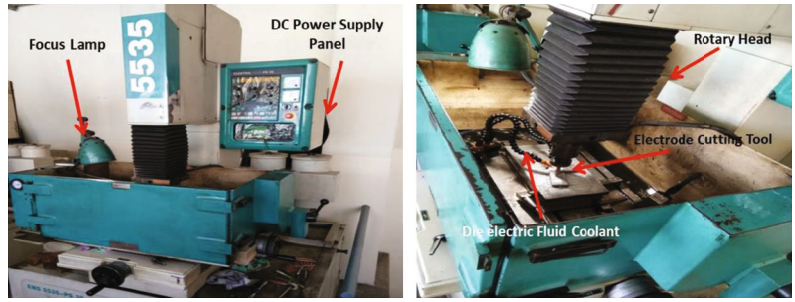

Figure 2: Elektra pulsPS35 die-sinking EDM.

Table 4: Process parameters with ranges and levels.

Factors	Unit	Ranges	Levels		
			1 (low)	2 (medium)	3 (high)
A	wt.% of RHA	6–10	W_1	W_2	W_3
B	A	5–15	5	10	15
C	V	50–80	50	65	80
D	%	8–24	8	16	24
E	μs	10–50	10	20	50
F	Psi	3–10	3	5	10

From the SN ratios graphs, the optimized value for better MRR, SR, and TWR are obtained at $A_1B_3C_3D_2E_3F_1$, $A_2B_1C_1D_2E_1F_3$, and $A_1B_1C_1D_1E_1F_3$, respectively.

3.2. Selection of Significant Parameters. To discover the parameters that are statistically significant for high MRR, low SR, and low TWR, an ANOVA tables have been constructed using the Minitab software. The ANOVA table generated for MRR, SR, and TWR are shown in Tables 7, 8 and 9, respectively. It is utilized to evaluate the significant parameters and indicates its importance towards the MRR, SR, and TWR. The probability (P) value in the ANOVA table should be less than 0.05 for the significant factor [38–42]. The complete outcome was validated at a 95% level of confidence; it was revealed that RHA content, discharge current, gap voltage, and duty factor have the significant influence on MRR. RHA content, discharge current, gap voltage, duty factor, and pulse-on time have the most significant effect on SR of machined specimens. RHA content and discharge current have most significance towards TWR. The coefficient of determination (R^2) for MRR, SR, and TWR are 96.36%, 94.65%, and 93.86%, respectively.

3.3. Prediction. The mean of optimal MRR, SR, and TWR is estimated at the significant level of machining factors at $A_1B_3C_3D_2E_3F_1$, $A_2B_1C_1D_2E_1F_3$, and $A_1B_1C_1D_1E_1F_3$, respectively. The predicted mean of the response parameters MRR, SR, and TWR is calculated [43, 44] using

$$\begin{aligned}\mu\text{MRR} &= \text{Workpiece} - \text{electrode1} + \text{Discharge} - \text{current3} \\ &\quad + \text{Gap} - \text{voltage3} + \text{Duty} - \text{factor2} + \text{Pulse} \\ &\quad - \text{on time3} + \text{Flushing} - \text{pressure1} - 5\text{Tavg} \\ &= 51.82 + 59.39 + 44.85 + 45.40 + 41.33 + 47.89 \\ &\quad - 5 \times 39.930 = 91.03\ \text{mg/min} \\ \mu\text{SR} &= \text{Workpiece} - \text{electrode2} + \text{Discharge} - \text{current1} \\ &\quad + \text{Gap} - \text{voltage1} + \text{Duty} - \text{factor2} + \text{Pulse} \\ &\quad - \text{on time1} + \text{Flushing} - \text{pressure3} - 5\text{Tavg} \\ &= 3.700 + 3.258 + 3.794 + 3.937 + 3.873 + 4.189 \\ &\quad - 5 \times 4.200 = 1.751\ \mu\text{m} \\ \mu\text{TWR} &= \text{Workpiece} - \text{electrode1} + \text{Discharge} - \text{current1} \\ &\quad + \text{Gap} - \text{voltage1} + \text{Duty} - \text{factor1} + \text{Pulse} \\ &\quad - \text{on time1} + \text{Flushing} - \text{pressure3} - 5\text{Tav} \\ &= 9.083 + 8.889 + 10.014 + 10.931 + 10.292 + 10.208 \\ &\quad - 5 \times 11.055 = 4.142\ \text{mg/min}\end{aligned} \tag{4}$$

3.4. Confirmatory Experiments. Finally, the confirmatory experiments are conducted to validate the optimal parametric combination. Three confirmatory tests for MRR, SR, and TWR are carried out at their optimal set process parameters, and their average value is compared with their corresponding estimated mean optimal value. Table 10 shows the results of confirmatory experiment for MRR, SR, and TWR produced by copper electrode. Confirmation experiments shows that results of trial at optimal conditions have shown improvement when compared with the results of trials at chosen initial setting of control parameters.

3.5. Micrographs of Machined Surfaces. The microstructure of the workpieces is studied by applying the SEM for evaluating the quality of surfaces produced by EDM process. The specimens were etched properly in a mixture of distilled water, HCl, and CuSO4 for 60 seconds before SEM observations [41, 42].

Analysis of micrographs has been performed of all the workpiece for low and high levels of discharge current. The two specimens from each workpiece are chosen for study

Table 5: Experimental results of EDM produced by copper electrode.

Exp. no.	A	B	C	D	E	F	Response values (average)			S/N ratio		
							MRR	SR	TWR	MRR	SR	TWR
1	6	5	50	8	10	3	32.125	3.26	3.625	11.1863	-10.2646	-9.8855
2	6	5	50	8	20	5	25.625	3.65	4.750	13.5340	-11.2461	-11.9412
3	6	5	50	8	30	10	23.125	4.16	2.875	9.1729	-12.3821	-12.7913
4	6	10	65	16	10	3	55.625	4.46	10.375	20.3199	-12.9869	-15.8278
5	6	10	65	16	20	5	48.375	4.75	7.625	17.6449	-13.5341	-18.1254
6	6	10	65	16	30	10	49.375	4.69	5.375	14.6077	-13.4238	-18.0140
7	6	15	80	24	10	3	82.125	5.19	12.750	22.1104	-14.3034	-20.9735
8	6	15	80	24	20	5	76.875	5.16	18.500	25.3438	-14.2531	-24.0249
9	6	15	80	24	30	10	73.125	6.46	15.875	24.0145	-16.2049	-25.1178
10	8	5	65	24	10	5	21.875	2.85	7.250	17.2069	-9.0969	-10.5178
11	8	5	65	24	20	10	20.625	3.30	7.375	17.3554	-10.3705	-9.6737
12	8	5	65	24	30	3	26.875	2.92	9.750	19.7801	-9.3078	-11.9661
13	8	10	80	8	10	5	30.625	3.77	9.500	19.5548	-11.5269	-12.5768
14	8	10	80	8	20	10	29.375	3.90	10.250	20.2149	-11.8215	-14.5288
15	8	10	80	8	30	3	46.875	4.21	10.750	20.6287	-12.4858	-16.5947
16	8	15	50	16	10	5	63.125	4.06	13.500	22.6069	-12.1707	-18.0246
17	8	15	50	16	20	10	46.875	3.92	14.500	23.22765	-11.8659	-19.6945
18	8	15	50	16	30	3	80.625	4.37	16.125	24.1500	-12.8099	-21.8441
19	10	5	80	16	10	10	23.000	2.56	7.875	17.9250	-8.1649	-9.4416
20	10	5	80	16	20	3	26.875	3.60	11.375	21.1190	-11.1263	-7.2067
21	10	5	80	16	30	5	14.750	3.02	7.125	17.0558	-9.6003	-12.5403
22	10	10	50	24	10	10	16.500	3.25	9.125	19.2049	-10.2379	-16.0219
23	10	10	50	24	20	3	31.750	3.65	12.875	22.1952	-11.2461	-14.3791
24	10	10	50	24	30	5	21.375	3.83	12.750	22.1104	-11.6642	-12.9796
25	10	15	65	8	10	10	26.625	5.46	18.625	25.4018	-14.7442	-16.7335
26	10	15	65	8	20	3	48.125	6.51	19.125	25.6323	-16.2719	-17.2923
27	10	15	65	8	30	5	35.875	6.46	18.875	25.5179	-16.2049	-17.5755

of microstructure. Figures 6–8 show the microstructure of the sample machined at experimental run-3, run-9, run-12, run-18, run-21, and run-27. This can be observed from the SEM micrographs that there is a formation of residual cavity, globules, and large deep craters on the surface of some specimens after machining. The possible cause of this may be high value of discharge current. Higher discharge energy creates higher temperatures at the spark point during EDM, which causes material to melt and evaporate. Figures 6, 7, and 8 confirmed that craters are shallow and surface imperfections are smooth, shallow, and less widespread at low discharge current. The melted material which is not properly flushed out from the surface is solidified again and formed a rougher surface which can be visualised in Figure 6. Higher discharge energy is available at higher discharge current and pulse-on time levels, which results in formation of large craters, microcracks, and debris. Riaz et al. also confirmed the deep craters and large surface irregularities surfaces at high discharge energy [43]. Further, it is clearly understood that material has undergone melting followed by washing out of the molten material. Suresh Kumar et al. claimed that a large proportion of the heat produced is dissipated in the machining area at a lower level of discharge current [44]. Hence, lesser pulse energy is dispensed for the melting and vaporization workpiece. The increase in pulse-on-time reduces machining efficiency. The machined surface is therefore present with the waviness surface and bubbles produced during pulse-off time, which might be due to collapse in plasma [45, 46].

4. Multiresponse Optimization Using GRA

4.1. Generating Grey Relational Grade. GRA analysis is employed here to optimize multiple responses, namely, MRR, SR, and TWR using single response value of EDM process of nanocomposites material. The various steps involved in calculating GRG are as follows.

Step 1. Calculate the mean for each individual corresponding response.

Step 2. Normalize the data in range between 0 and 1 using the following formulae.

Table 6: Response for means of MRR, SR, and TWR.

	MRR						SR						TWR					
Levels	A	B	C	D	E	F	A	B	C	D	E	F	A	B	C	D	E	F
1	51.82	23.88	37.90	33.15	39.07	47.89	4.642	3.258	3.794	4.598	3.873	4.241	9.083	8.889	10.014	10.931	10.292	11.861
2	40.76	36.65	37.04	45.40	39.39	37.61	3.700	4.057	4.600	3.937	4.271	4.172	11.000	9.847	11.597	10.431	11.819	11.097
3	27.21	59.26	44.85	41.24	41.33	34.29	4.260	5.288	4.208	4.068	4.458	4.189	13.083	16.431	11.556	11.806	11.056	10.208
Delta	24.61	35.39	7.81	12.25	2.26	13.60	0.942	2.030	0.806	0.661	0.584	0.069	4.000	9.542	1.583	1.375	1.528	1.653
Rank	2	1	5	4	6	3	2	1	3	4	5	6	2	1	4	6	5	3

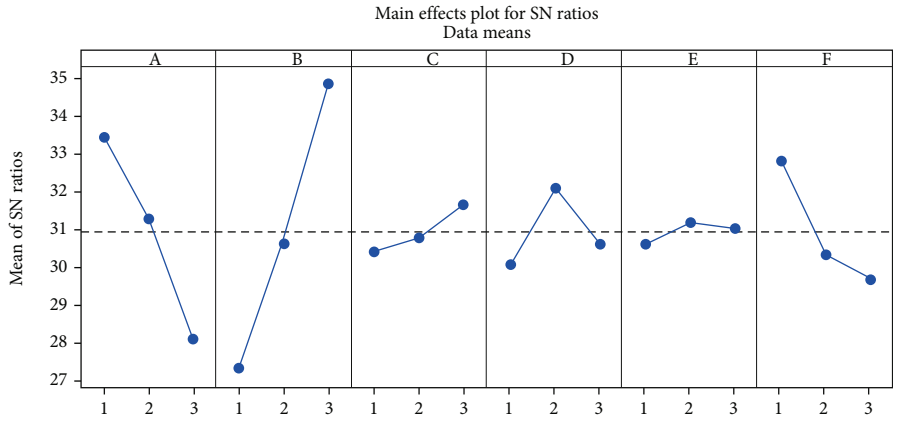

Signal-to-noise: Larger is better

Figure 3: Main effect plots for SN ratios of MRR.

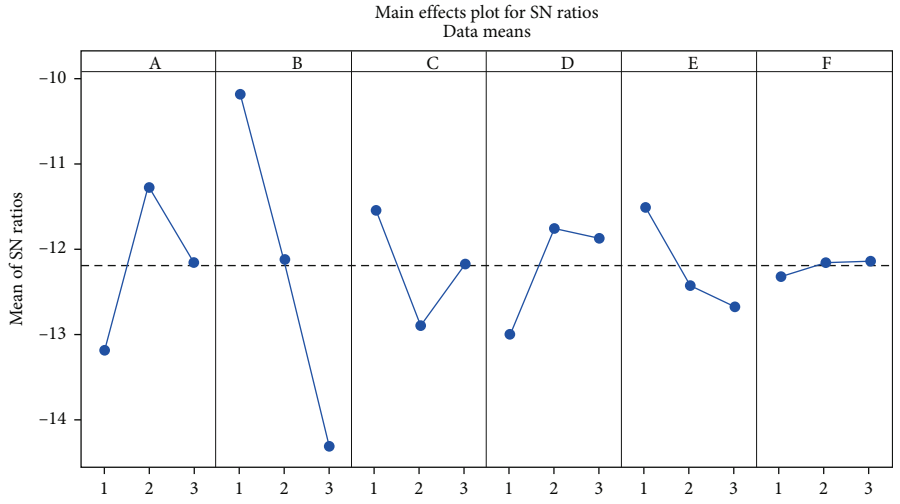

Signal-to-noise: Smaller is better

Figure 4: Main effect plots for SN ratios of SR.

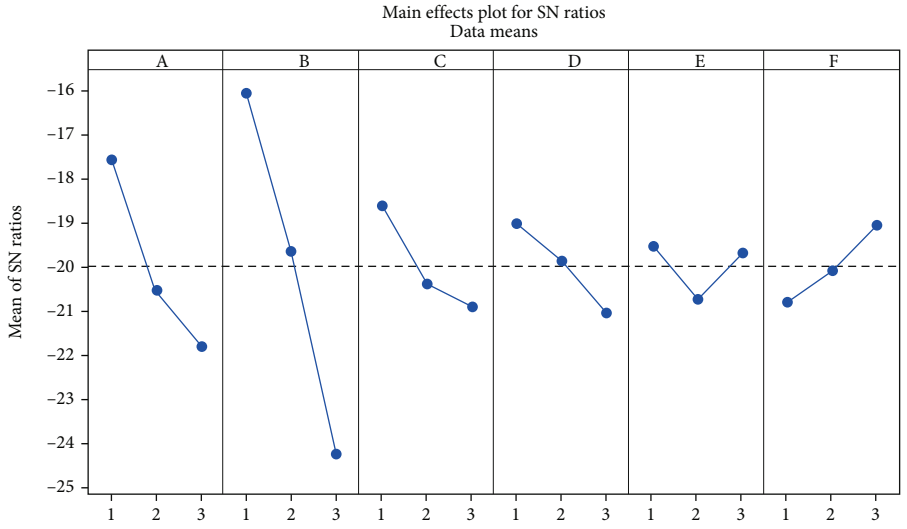

Signal-to-noise: Smaller is better

Figure 5: Main effect plots for SN ratio of TWR.

Table 7: ANOVA for MRR.

Source	DOF	Adj. SS	Adj. MS	F value	P value	% Contribution
A: Workpiece electrode	2	2735.1	1367.53	48.32	≤0.001	25.158
B: Discharge current	2	5780.7	2890.36	102.13	≤0.001	53.172
C: Gap voltage	2	329.7	164.84	5.82	0.014	3.033
D: Duty factor	2	698.3	349.51	12.34	0.001	6.423
E: Pulse-on time	2	27.0	13.51	0.48	0.630	0.248
E: Flushing pressure	2	904.6	452.30	15.98	≤0.001	8.321
Error	14	394.2		28.30		
Total	26			10871.6		

$S = 5.31993$, $R - \text{sq.} = 96.36\%$, $R - \text{sq.(adj.)} = 93.235\%$, and $R - \text{sq.(pred.)} = 86.442\%$.

Table 8: ANOVA for SR.

Source	DOF	Adj. SS	Adj. MS	F value	P value	% Contribution
A: Workpiece electrode	2	4.0424	2.02121	16.89	≤0.001	12.916%
B: Discharge current	2	18.8243	9.41214	78.67	≤0.001	60.150%
C: Gap voltage	2	2.9208	1.46040	12.21	0.001	9.333%
D: Duty factor	2	2.2055	1.10274	9.22	0.003	7.047%
E: Pulse-on time	2	1.6039	0.80197	6.70	0.009	5.125%
E: Flushing pressure	2	0.0233	0.01163	0.10	0.908	0.074%
Error	14	1.6750	0.11964			
Total	26	31.2952				

$S = 0.345895$, $R - \text{sq.} = 94.65\%$, $R - \text{sq.(adj.)} = 90.0612\%$, and $R - \text{sq.(pred.)} = 80.098\%$.

Table 9: ANOVA for TWR.

Source	DOF	Adj. SS	Adj. MS	F value	P value	% Contribution
A: Workpiece electrode	2	72.042	36.021	14.07	≤0.001	12.347
B: Discharge current	2	429.406	214.703	83.88	≤0.001	73.594
C: Gap voltage	2	14.656	7.328	2.86	0.091	2.512
D: Duty factor	2	8.719	4.359	1.70	0.218	1.494
E: Pulse-on time	2	10.503	5.252	2.05	0.165	1.800
F: Flushing pressure	2	12.316	6.158	2.41	0.126	2.111
Error	14	35.837		2.560		
Total	26			583.479		

$S = 1.59993$, $R^2 = 93.861\%$, R^2 (adj.) $= 88.592\%$, R^2 (pred.) $= 77.161\%$.

Table 10: Results of confirmatory experiment for MRR, SR, and TWR.

Machining characteristics	Predicted optimum value	Predicted confidence interval at 95% confidence level	Optimal set of machining parameters	Experimental value (mg/min)
MRR	91.031 mg/min	$80.721 < \mu_{\text{MRR-Cu}} < 101.339$	$A_1B_3C_3D_2E_3F_1$	87.151
SR	1.753 μm	$1.065 < \mu_{\text{SR-cu}} < 2.403$	$A_2B_1C_1D_2E_1F_3$	1.912
TWR	4.141 mg/min	$1.044 < \mu_{\text{TWR-Cu}} < 7.24$	$A_1B_1C_1D_1E_1F_3$	4.892

For higher the better,

$$x_i * (k) = \frac{x_i(k) - \min x_i(k)}{\max x_i(k) - \min x_i(k)}. \quad (5)$$

For smaller the better, the formula to transform $x_i(k)$ to $x_i * (k)$ is given as

$$x_i * (k) = \frac{\max x_i(k) - x_i(k)}{\max x_i(k) - \min x_i(k)} \quad (6)$$

(For $i = 1, 2, 3, \cdots$m and $k = 1, 2, 3, \cdots$n.)

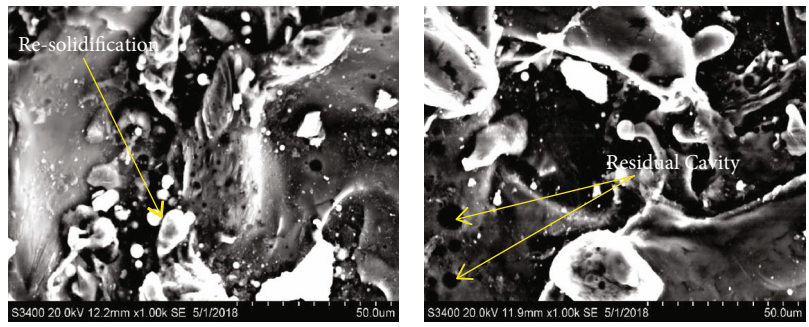

(a) (b)

Figure 6: SEM of workpiece W_1 at (a) current 5 Amp, gap voltage 50 V, duty factor 8%, pulse-on time 30 μs, and flushing pressure 10 psi and (b) run 9, current 15 Amp, gap voltage 80 V, duty factor 24%, pulse-on time 30 μs, and flushing pressure 10 psi.

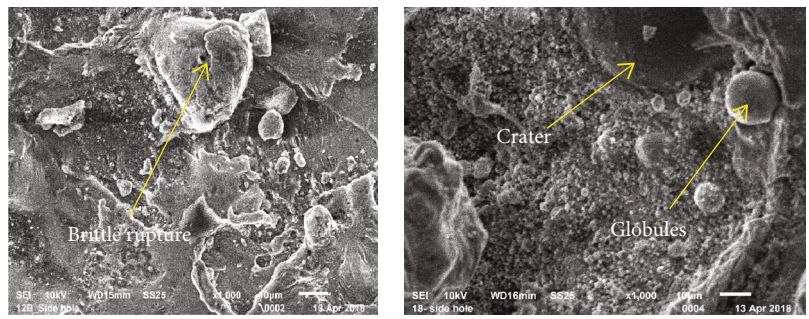

(a) (b)

Figure 7: SEM of workpiece W_2 at (a) current 5 Amp, gap voltage 65 V, duty factor 24%, pulse-on time 30 μs, and flushing pressure 3 psi and (b) current 15 Amp, gap voltage 50 V, duty factor 16%, pulse-on time 30 μs, and flushing pressure 3 psi.

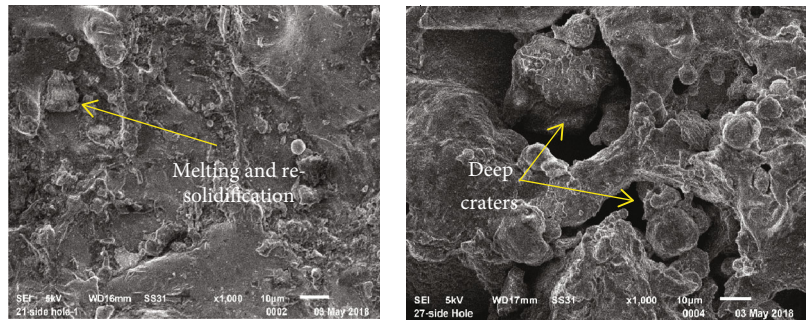

(a) (b)

Figure 8: SEM of workpiece W_3 at (a) current 5 Amp, gap voltage 80 V, duty factor 16%, pulse-on time 30 μs, and flushing pressure 5 psi and (b) current 15 Amp, gap voltage 65 V, duty factor 8%, pulse-on time 30 μs, and flushing pressure 5 psi.

where $x_i^*(k)$ is the string after the calculations, $i = 1, 2, 3 \cdots .m$, $m = 27$, and max x_i and min x_i are the functions for finding the maximum and minimum value of x_i^0, respectively.

Step 3. Calculate the divergence values from the normalized values, which is calculated using the formulae.

The deviation series $\Delta x_{oi}(k)$ is the difference of reference series $x_0 * (k)$ and the comparability series $x_i * (k)$ at k^{th} point.

It is computed using the following:

$$\Delta_{oi}(k) = |x_0(k) - x_i(k)| \tag{7}$$

Step 4. Determinate Grey relational coefficients (GRC).

Table 11: Grey relational grade.

Sr. no.	Normalized value			Divergence			Grey relational coefficient			GRG
	MRR	SR	TWR	MRR	SR	TWR	MRR	SR	TWR	
1	0.258	0.823	0.954	0.742	0.177	0.046	0.3501	0.6292	0.8672	0.615
2	0.161	0.724	0.885	0.839	0.276	0.115	0.3234	0.5211	0.7223	0.522
3	0.124	0.595	1.000	0.876	0.405	0.000	0.3146	0.4252	1.0001	0.580
4	0.607	0.519	0.538	0.393	0.481	0.462	0.504	0.384	0.394	0.427
5	0.499	0.446	0.708	0.501	0.554	0.292	0.444	0.351	0.506	0.434
6	0.514	0.461	0.846	0.486	0.539	0.154	0.451	0.357	0.661	0.490
7	1.000	0.334	0.392	0.000	0.666	0.608	1.000	0.311	0.331	0.547
8	0.922	0.342	0.038	0.078	0.658	0.962	0.837	0.313	0.238	0.463
9	0.866	0.013	0.200	0.134	0.987	0.800	0.750	0.233	0.273	0.418
10	0.106	0.927	0.731	0.894	0.073	0.269	0.309	0.803	0.527	0.546
11	0.087	0.813	0.723	0.913	0.187	0.277	0.305	0.616	0.520	0.480
12	0.180	0.909	0.577	0.820	0.091	0.423	0.328	0.767	0.415	0.503
13	0.236	0.694	0.592	0.764	0.306	0.408	0.344	0.495	0.424	0.421
14	0.217	0.661	0.546	0.783	0.339	0.454	0.338	0.469	0.398	0.402
15	0.477	0.582	0.515	0.523	0.418	0.485	0.433	0.418	0.382	0.411
16	0.718	0.620	0.346	0.282	0.380	0.654	0.587	0.441	0.315	0.447
17	0.477	0.656	0.285	0.523	0.344	0.715	0.433	0.466	0.295	0.398
18	0.978	0.542	0.185	0.022	0.458	0.815	0.947	0.396	0.269	0.537
19	0.122	1.000	0.692	0.878	0.000	0.308	0.313	1.000	0.494	0.602
20	0.180	0.737	0.477	0.820	0.263	0.523	0.328	0.533	0.364	0.408
21	0.000	0.884	0.738	1.000	0.116	0.262	0.286	0.720	0.534	0.513
22	0.026	0.825	0.615	0.974	0.175	0.385	0.291	0.632	0.438	0.454
23	0.252	0.724	0.385	0.748	0.276	0.615	0.349	0.521	0.328	0.399
24	0.098	0.678	0.392	0.902	0.322	0.608	0.307	0.483	0.331	0.373
25	0.176	0.266	0.031	0.824	0.734	0.969	0.3277	0.2902	0.2361	0.284
26	0.495	0.000	0.000	0.505	1.000	1.000	0.4425	0.2313	0.2312	0.301
27	0.314	0.013	0.015	0.686	0.987	0.985	0.3683	0.2334	0.2341	0.278

The GRC (ξ) is used to compute the relationship between mean and best values as follows:

$$\xi_{0i}(k) = \frac{\Delta \min + p\Delta \max}{\Delta_{oi}(k) + p\Delta \max} \tag{8}$$

Step 5. Generate the GRG.

Once the GRC is derived, the GRG is taken as the mean of GRC and is determined using following equations:

$$r_i = \frac{1}{n}\sum_{k=1}^{n}[w(k)\xi(k)] \tag{9}$$

$$\sum_{k=1}^{n} w(k) = 1 \tag{10}$$

In Equation (9), $w(k)$ is the ratio of the number k influencing parameter to the overall influencing indicators, and its overall sum is equal to 1.

Table 12: Response table for means of GRG.

Level	A	B	C	D	E	F
1	0.4996	0.5301	0.4807	0.4238	0.4828	0.4611
2	0.4607	0.4235	0.4161	0.4731	0.4230	0.4443
3	0.4016	0.4083	0.4651	0.4649	0.4561	0.4565
Delta	0.0980	0.1218	0.0646	0.0493	0.0597	0.0168
Rank	2	1	3	5	4	6

4.2. Selection of Optimal Levels. It can be observed from the Table 11 that the highest GRG is found at experimental trial no. 1 and optimum parametric combinations are as workpiece electrode W_1 (6%RHA), discharge current 5 A, gap voltage 65 V, duty factor 8%, pulse-on time 10 μs, and flushing pressure 3 psi. GRG is treated as an output variable on which subsequent optimisation is performed. Table 12 presents the mean GRG obtained for three different levels of EDM process variables. The overall mean value obtained of the GRG for 27 experiments is 0.454. Figures 9 and 10 present the main effects for mean and SN ratios of GRG for MRR, SR, and TWR produced by copper electrode. The

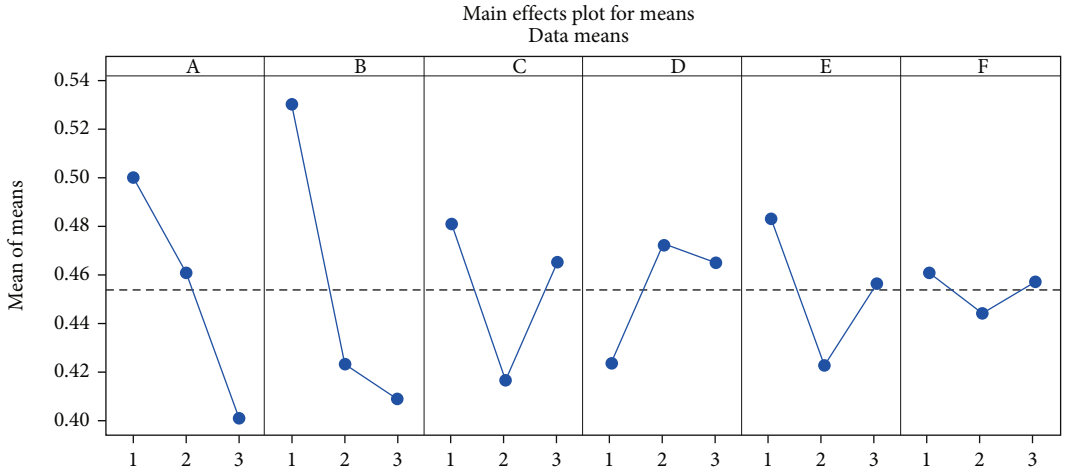

Figure 9: Main effects plot of Mean of GRG.

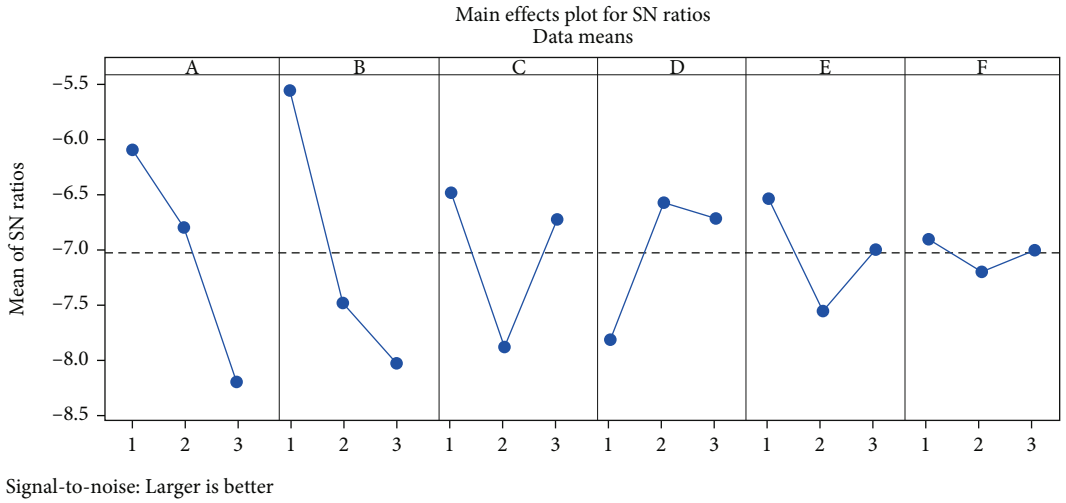

Figure 10: Main effects plot of SN ratios of GRG.

Table 13: ANOVA table for multiresponse characteristics GRG.

Source	DOF	Adj. SS	Adj. MS	F value	P value	% Contribution
A: Workpiece electrode	2	0.043836	0.021918	9.37	0.003	21.2482
B: Discharge current	2	0.079253	0.039626	16.94	≤0.001	38.4155
C: Gap voltage	2	0.020432	0.010216	4.37	0.034	9.9046
D: Duty factor	2	0.012553	0.006276	2.68	0.103	6.0852
E: Pulse-on time	2	0.016125	0.008063	3.45	0.061	7.8161
E: Flushing pressure	2	0.001365	0.000682	0.29	0.751	0.6621
Error	14	0.032744		0.002339		
Total	26			0.206307		

$S = 0.04836142$, $R^2 = 84.131\%$, R^2 (adj.) = 70.521%, and R^2 (pred.) = 40.977%.

optimal machining performance for multiple responses of EDM is $A_1B_1C_1D_2E_1F_1$ machined using copper electrode (i.e., workpiece electrode (level 1, GRG = 0.4996), discharge current (level 1, GRG = 0.5301), gap voltage (level 1, GRG = 0.4807), duty factor (level 2, GRG = 0.4731), pulse-on time (level 1, GRG = 0.4828), and flushing pressure (level 1, GRG = 0.4611)]. Table 13 shows the ANOVA results for multiresponse characteristics GRG for 27 different experiments. ANOVA results establish that workpiece electrode (RHA content), discharge current, and gap voltage are most significant parameters with contribution of 21.248%, 38.415%, and 9.904%, respectively.

5. Conclusions

The present study reveals the possibility of RHA; an agro-waste is reinforcement for fabrication of aluminium matrix hybrid nanocomposites to improve the mechanical properties of Al 6061 alloy and optimization of the EDM process using the copper electrode. Based on the fabrication and experimental investigations of hybrid Al/(RHA+Mg+Cu)-MMNCs, the following conclusions have been drawn:

(i) The hybrid 90 wt.% Al6061+6wt.%RHA+3 wt.% Cu +1 wt.% Mg, 88 wt.% Al6061+8 wt.% RHA+3 wt.% Cu+1 wt.% Mg, and 86 wt.% Al6061+10 wt.% RHA +3 wt.% Cu+1wt.%Mg MMC can be fabricated using liquid stir casting

(ii) The optimal parametric combinations for response characteristics, i.e., MRR, SR, and TWR, for the hybrid 90 wt.% Al6061+6wt.%RHA+3 wt.% Cu +1 wt.% Mg, 88 wt.% Al6061+8 wt.% RHA+3 wt.% Cu+1 wt.% Mg, and 86 wt.% Al6061+10 wt.% RHA +3 wt.% Cu+1wt.%Mg MMC are A1B3C3D2E3F1, A2B1C1D2E1F2, and A1B1C1D1E1F3, respectively, when machining experiments were performed using copper as tool electrode

(iii) The predicted interval of response characteristics, i.e., MRR, SR, and TWR, using optimum levels of EDM parameters parameter when machining operations are carried out with copper electrode is $80.721 < \mu_{MRR} < 101.339$, $1.065 < \mu_{SR} < 2.403$, and $1.044 < \mu_{TWR} < 7.24$, respectively

(iv) The validity experiments confirmed that the average values of response characteristics, i.e., MRR, SR, and TWR, obtained at optimal level of EDM parameters fall within the predicted confidence interval at 95% confidence level

(v) The GRA is used for simultaneous optimization of the MRR, SR, and TWR. The confirmation experiments for optimal parametric setting as determined using response graph for GRG show improvement over initial parametric setting of machining parameters for all material combination selected for experimental investigation

Data Availability

The data presented in this study are available on request from the corresponding author.

Conflicts of Interest

The authors declare that they have no conflicts of interest.

References

[1] R. K. Garg, K. K. Singh, A. Sachdeva, V. S. Sharma, K. Ojha, and S. Singh, "Review of research work in sinking EDM and WEDM on metal matrix composite materials," *The International Journal of Advanced Manufacturing Technology*, vol. 50, no. 5-8, pp. 611–624, 2010.

[2] A. Hasçalık and U. Çaydaş, "Optimization of turning parameters for surface roughness and tool life based on the Taguchi method," *The International Journal of Advanced Manufacturing Technology*, vol. 38, no. 9-10, pp. 896–903, 2008.

[3] S. Arif, T. Alam, A. H. Ansari, and M. B. Shaikh, "Morphological characterization, statistical modelling and tribological behaviour of aluminum hybrid nanocomposites reinforced with micro-nano-silicon carbide," *Journal of Asian Ceramic Societies*, vol. 7, no. 4, pp. 434–448, 2019.

[4] N. K. Bhoi, H. Singh, and S. Pratap, "Developments in the aluminum metal matrix composites reinforced by micro/nano particles – a review," *Journal of Composite Materials*, vol. 54, no. 6, pp. 813–833, 2019.

[5] K. K. Alaneme and P. A. Olubambi, "Corrosion and wear behaviour of rice husk ash–Alumina reinforced Al-Mg-Si alloy matrix hybrid composites," *Journal of Materials Research and Technology*, vol. 2, no. 2, pp. 188–194, 2013.

[6] M. B. Shaikh, S. Raja, M. Ahmed, M. Zubair, A. Khan, and M. Ali, "Rice husk ash reinforced aluminium matrix composites: fabrication, characterization, statistical analysis and artificial neural network modelling," *Materials Research Express*, vol. 6, no. 5, article 056518, 2019.

[7] P. Mishra, P. Mishra, and R. S. Rana, "Effect of rice husk ash reinforcements on mechanical properties of aluminium alloy (LM6) matrix composites," *Materials Today: Proceedings*, vol. 5, pp. 6018–6022, 2019.

[8] H. M. Zakaria, "Microstructural and corrosion behavior of Al/SiC metal matrix composites," *Ain Shams Engineering Journal*, vol. 5, no. 3, pp. 831–838, 2014.

[9] S. Hossain, M. D. M. Rahman, D. Chawla et al., "Fabrication, microstructural and mechanical behavior of Al-Al2O3-SiC hybrid metal matrix composites," *Materials Today: Proceedings*, vol. 21, pp. 1458–1461, 2020.

[10] D. K. Sharma, D. Mahant, and G. Upadhyay, "Manufacturing of Metal Matrix Composites: A State of Review," *Materials Today: Proceedings*, vol. 26, pp. 506–519, 2020.

[11] S. Sharma, J. Singh, M. K. Gupta et al., "Investigation on mechanical, tribological and microstructural properties of Al-Mg-Si-T6/SiC/muscovite-hybrid metal-matrix composites for high strength applications," *Journal of Materials Research and Technology*, vol. 12, no. 21, pp. 1564–1581, 2021.

[12] I. Dinaharan, K. Kalaiselvan, E. T. Akinlabi, and J. Paulo Davim, "Microstructure and wear characterization of rice husk ash reinforced copper matrix composites prepared using friction stir processing," *Journal of Alloys and Compounds*, vol. 718, pp. 150–160, 2017.

[13] A. K. Srivastava, "Assessment of mechanical properties and EDM machinability on Al6063/SiC MMC produced by stir casting," *Materials Today: Proceedings*, vol. 25, pp. 630–634, 2020.

[14] J. Kumar, D. Singh, N. S. Kalsi et al., "Investigation on the mechanical, tribological, morphological and machinability behavior of stir-casted Al/SiC/Mo reinforced MMCs," *Journal of Materials Research and Technology*, vol. 12, pp. 930–946, 2021.

[15] R. G. Rao, M. Ghosh, R. I. Ganguly, and K. L. Sahoo, "Mechanical properties and age hardening response of Al6061 alloy based composites reinforced with fly ash," *Materials Science and Engineering*, vol. 772, article 138823, 2020.

[16] R. N. Muni, J. Singh, V. Kumar, and S. Sharma, "Influence of rice husk ash, Cu, Mg on the mechanical behaviour of aluminium matrix hybrid composites," *International Journal of Applied Engineering Research*, vol. 14, no. 8, pp. 1828–1834, 2019.

[17] A. K. Virkunwar, S. Ghosh, and R. Basak, "Friction Performance Optimization of Al6061-Rice Husk Ash Metal Matrix Composite Using Taguchi Method," *Materials Today: Proceedings*, vol. 19, pp. 415–419, 2019.

[18] A. K. Virkunwar, S. Ghosh, and R. Basak, "Wear Characteristics Optimization of Al6061-Rice Husk Ash Metal Matrix Composite Using Taguchi Method," *Materials Today: Proceedings*, vol. 19, pp. 546–550, 2019.

[19] J. Li and R. A. Laghari, "a review on machining and optimization of particle-reinforced metal matrix composites," *International Journal of Advanced Manufacturing Technology*, vol. 100, no. 9-12, pp. 2929–2943, 2019.

[20] V. Bharath, N. Madev, V. Auradi, and S. A. Kori, "Preparation of 6061Al-Al2O3 MMC's by stir casting and evaluation of mechanical and wear properties," *Procedia Materials Science*, vol. 6, pp. 1658–1667, 2014.

[21] B. M. Schumacher, R. Krampitz, and J. P. Kruth, "Historical phases of EDM development driven by the dual influence of market pull and science push," *Procedia CIRP*, vol. 6, pp. 5–12, 2013.

[22] M. B. Shaikh, S. Arif, and M. A. Siddiqui, "Fabrication and characterization of aluminium hybrid composites reinforced with fly ash and silicon carbide through powder metallurgy," *Materials Research Express*, vol. 5, no. 4, article 046506, 2018.

[23] P. Ravindran, K. Manisekar, S. Vinoth Kumar, and P. Rathika, "Investigation of microstructure and mechanical properties of aluminum hybrid nano-composites with the additions of solid lubricant," *Materials and Design*, vol. 51, pp. 448–456, 2013.

[24] K. K. Alaneme, T. M. Adewale, and P. A. Olubambi, "Corrosion and wear behaviour of Al–Mg–Si alloy matrix hybrid composites reinforced with rice husk ash and silicon carbide," *Journal of Materials Research and Technology*, vol. 3, no. 1, pp. 9–16, 2014.

[25] K. K. Alaneme and K. O. Sanusi, "Microstructural characteristics, mechanical and wear behaviour of aluminium matrix hybrid composites reinforced with alumina, rice husk ash and graphite," *Engineering Science and Technology, an International Journal*, vol. 18, no. 3, pp. 416–422, 2015.

[26] G. Arora and S. Sharma, "A comparative study of AA6351 mono-composites reinforced with synthetic and agro waste reinforcement," *International Journal of Precision Engineering and Manufacturing*, vol. 19, no. 4, pp. 631–638, 2018.

[27] K. Amouri, S. Kazemi, A. Momeni, and M. Kazazi, "Microstructure and mechanical properties of Al-nano/micro SiC composites produced by stir casting technique," *Materials Science and Engineering A*, vol. 674, pp. 569–578, 2016.

[28] A. Ramanathan, P. K. Krishnan, and R. Muraliraja, "A review on the production of metal matrix composites through stir casting – furnace design, properties, challenges, and research opportunities," *Journal of Manufacturing Processes*, vol. 42, pp. 213–245, 2019.

[29] A. Kumar and M. Kumar, "Mechanical and dry sliding wear behaviour of B_4C and rice husk ash reinfroced Al 7075 alloy hybrid composite for armors application by using taguchi techniques," *Materials Today: Proceedings*, vol. 27, pp. 2617–2625, 2020.

[30] R. N. Muni, J. Singh, V. Kumar, and S. Sharma, "Parametric optimization of rice husk ash, copper, magnesium reinforced aluminium matrix hybrid composite processed by EDM," *ARPN Journal of Engineering and Applied Sciences*, vol. 14, no. 22, 2019.

[31] S. P. Dwivedi, A. Saxena, and S. Sharma, "Influence of Nano-CuO on synthesis and mechanical behavior of spent alumina catalyst and grinding sludge reinforced aluminum based composite," *International Journal of Metalcasting*, vol. 16, no. 1, pp. 292–303, 2022.

[32] S. P. Dwivedi, A. Saxena, S. Sharma, A. K. Srivastava, and N. K. Maurya, "Influence of SAC and eggshell addition in the physical, mechanical and thermal behaviour of Cr reinforced aluminium based composite," *International Journal of Cast Metals Research*, vol. 34, no. 1, pp. 43–55, 2021.

[33] S. P. Dwivedi, R. Agrawal, and S. Sharma, "Effect of friction stir process parameters on mechanical properties of chrome containing leather waste reinforced aluminium based composite," *International Journal of Precision Engineering and Manufacturing-Green Technology*, vol. 8, no. 3, pp. 935–943, 2021.

[34] N. V. Rengasamy, M. Rajkumar, and S. Senthil Kumaran, "An analysis of mechanical properties and optimization of EDM process parameters of Al 4032 alloy reinforced with Zrb2 and Tib2 in-situ composites," *Journal of Alloys and Compounds*, vol. 662, no. 2016, pp. 325–338, 2016.

[35] B. C. Kandpal, J. Kumar, and H. Singh, "Optimization of electrical discharge machining AA6061/ 10 %Al_2O_3 composite using Taguchi optimization technique," *Materials Today: Proceedings*, vol. 5, pp. 18946–18955, 2018.

[36] S. Dhar, R. Purohit, N. Saini, A. Sharma, and K. G. Hemath, "Mathematical modeling of electric discharge machining of cast Al-4Cu-6Si alloy-10 wt.% SiC_P composites," *Journal of Materials Processing Technology*, vol. 194, no. 1-3, pp. 24–29, 2007.

[37] A. K. Bodukuri, S. Chandramouli, K. Eswaraiah, and J. Laxman, "Experimental Investigation and Optimization of EDM Process Parameters on Aluminum Metal Matrix Composite," *Materials Today: Proceedings*, vol. 5, pp. 24731–24740, 2018.

[38] S. Sharma and P. Sudhakara, "Fabrication and optimization of hybrid AA-6082-T6 alloy/8%Al_2O_3(alumina)/2%Grp metal matrix composites using novel Box-Behnken methodology processed by wire-sinking electric discharge machining," *Materials Research Express*, vol. 6, no. 11, article 116594, 2019.

[39] P. J. Ross, *Taguchi Techniques for Quality Engineering*, McGraw-Hills Book Company, New York, 1988.

[40] R. K. Roy, *A Primer on Taguchi Method*, Van Nostrand Reinhold, New York, 1990.

[41] J. Kumar, D. Singh, N. S. Kalsi et al., "Comparative study on the mechanical, tribological, morphological and structural properties of vortex casting processed, Al-SiC-Cr hybrid metal matrix composites for high strength wear-resistant applications: fabrication and characterizations," *Journal of Materials Research and Technology*, vol. 9, no. 6, pp. 13607–13615, 2020.

[42] S. P. Dwivedi, A. Saxena, S. Sharma et al., "Effect of ball-milling process parameters on mechanical properties of Al/Al_2O_3/collagen powder composite using statistical approach," *Journal of Materials Research and Technology*, vol. 15, pp. 2918–2932, 2021.

[43] A. Riaz, A. P. Ahamed, and S. Aravindan, "EDM of hybrid Al–SiCp–B4Cp and Al–SiCp–Glassp MMCs," *The International*

Journal of Advanced Manufacturing Technology, vol. 44, no. 56, pp. 520–528, 2009.

[44] S. Suresh Kumar, M. Uthayakumar, S. Thirumalai Kumaran, P. Parameswaran, and E. Mohandas, "Electrical discharge machining of Al (6351)-5% SiC-10% B4C hybrid composite: a Grey relational approach," *Modelling and Simulation in Engineering*, vol. 2014, 7 pages, 2014.

[45] S. V. Alagarsamy, M. Ravichandran, S. Dinesh Kumar, S. Sakthivelu, M. Meignanamoorthy, and C. Chanakyan, "A Taguchi coupled desirability function analysis of wire cut EDM behaviour of titanium dioxide filled aluminium matrix composite," *Materials Today: Proceedings*, vol. 27, pp. 853–858, 2020.

[46] S. S. Sidhu, A. Batish, and S. Kumar, "ED Machining of Particulate Reinforced MMC's," *International Journal of Industrial and Manufacturing Engineering*, vol. 8, no. 3, pp. 503–509, 2014.